Iranian Journal of Science & Technology, Transaction B: Engineering, Vol. 34, No. B2, pp 215-230
Printed in The Islamic Republic of Iran, 2010

ROTOR MASS EFFECT ON NONLINEAR DYNAMIC BEHAVIOR OF AERODYNAMIC NONCIRCULAR JOURNAL BEARING SYSTEMS*

R. RASHIDI[1],** A. KARAMI MOHAMMADI[1] AND F. BAKHTIARINEJAD[2]

[1]Dept. of Mechanical Engineering, Shahrood University of Technology, Shahrood, I. R. of Iran
Email: rrashidim@gmail.com
[2]Dept. of Mechanical Engineering, Amirkabir University of Technology, Tehran, I. R. of Iran

Abstract– This paper presents the effect of rotor mass on nonlinear dynamic behavior of a rigid rotor supported by aerodynamic noncircular journal bearings. A finite element method has been employed to solve the Reynolds equation in static and dynamical states and the dynamical equations are solved using Runge-Kutta method. To analyze the behavior of the rotor center in horizontal and vertical directions under different operating conditions, dynamic trajectory, power spectra, Poincare maps and bifurcation diagrams are used. Results of this study reveal how the complex dynamic behavior of two types of noncircular bearing systems comprising periodic and KT -periodic responses of the rotor center varies with changes in rotor mass values.

Keywords– Aerodynamic noncircular bearing, rotor mass, poincare map, bifurcation

1. INTRODUCTION

During the past few decades aerodynamic journal bearings have received great attention from practical and analytical tribologists. The rapid growth of gas bearing technology is mainly due to its wide range of engineering applications such as precision machine tools, high speed aircraft, nuclear reactors, textile spindles, dental drills, etc. Aerodynamic journal bearings have the advantage of negligible friction, cleanliness and easy availability of air as the lubricant, however poor dynamic stability due to low viscosity is a major problem. Therefore, investigation of dynamical behavior is necessary to avoid settling of the system in a region that has severe control.

In 1961, Castelli and Elrod [1] made a significant contribution towards a better understanding of the complex fluid dynamic phenomenon in gas lubrication. These authors presented their assessment of the validity of the assumptions made in the analysis of earlier investigators. They neglected the pressure time derivative term in the Reynolds equation and obtained the rotor center orbits for a specified set of operating and initial conditions by numerical integration of the equations of motion of the rotor.

Ausman [2] solved the linearized Reynolds equation of self acting bearings to investigate the stability of the static equilibrium position of the rotor. In 1978, Holmes et al. [3] discussed aperiodic behavior in short journal bearings. They noted that a moderate level of unbalance and a high eccentricity ratio led to an aperiodic response of the shaft at speeds above a critical threshold value. Chandra et al. [4] studied static and dynamic characteristics of four gas-lubricated noncircular journal bearing configurations. In their work, linearized Reynolds equation was solved by finite element method and comparative stability of four gas-lubricated noncircular journal bearing configurations was done.

In 1994, Zhao et al. [5] investigated nonlinear dynamic behavior of an eccentric squeeze film damper mounted rigid rotor system. The authors showed that for large values of unbalance and static

*Received by the editors April 17, 2009; Accepted October 13, 2009.
**Corresponding author

misalignment, the sub-harmonic and quasi-periodic motions generated at speeds of more than twice the system critical speed were bifurcated from the unbalanced harmonic solution.

Nonlinear dynamic behavior such as sub-harmonic, quasi-periodic and chaotic motions for suitable values of system parameters in a rigid rotor supported by short bearings were reported by Adiletta et al. through theoretical and experimental investigations [6-8]. Czolczynski and Kapitaniak [9] described a method which allows the control of the Hopf bifurcation of a rotor system supported by two gas bearings. They showed the damage caused by the growing amplitude of self excited vibrations can be avoided by a proper selection of stiffness and damping coefficients of the air ring.

Nonlinear dynamic and bifurcation analysis of a rigid rotor [10] and a flexible rotor [11] supported by a self-acting gas journal bearing were studied by Wang et al. In both works, by considering rotor mass and rotational speed as the parameters of the system, periodic and sub-harmonic motions of the rotor center were reported. In 2005, Wang Jiun-Shen and Wang Cheng-Chi [12] presented bifurcation of a rigid rotor by relative short aerodynamic journal bearings. They discussed how the existence of a complex dynamic behavior comprises periodic and sub-harmonic responses of the rotor center. Also, Wang [13] provided a further understanding of a rigid rotor supported by a relatively short externally pressurized porous gas journal bearing and showed the dynamic behavior of the system with respect to rotor mass and bearing number.

In 2007, Wang et al. studied the behavior of a rigid rotor [14] and a flexible rotor [15] supported by a herringbone-grooved gas journal bearing system. Their analysis revealed a complex dynamic behavior comprising periodic and quasi-periodic responses of the system. Rahmatabadi and Rashidi investigated static and dynamic characteristics of noncircular gas-lubricated journal bearings by considering the effect of mount angle [16] and preload [17]. They showed noncircular bearings have better dynamic characteristics than circular bearings. Also, by using a suitable value of mount angle, the stability margin can be increased.

Although previous works provide insight into the behavior of the system, the bifurcation and nonlinear dynamic behavior of the aerodynamic noncircular journal bearing has not been examined. Therefore, this paper presents the effect of rotor mass on nonlinear dynamic behavior of a rigid rotor supported by two and three-lobe bearings (Fig. 1).

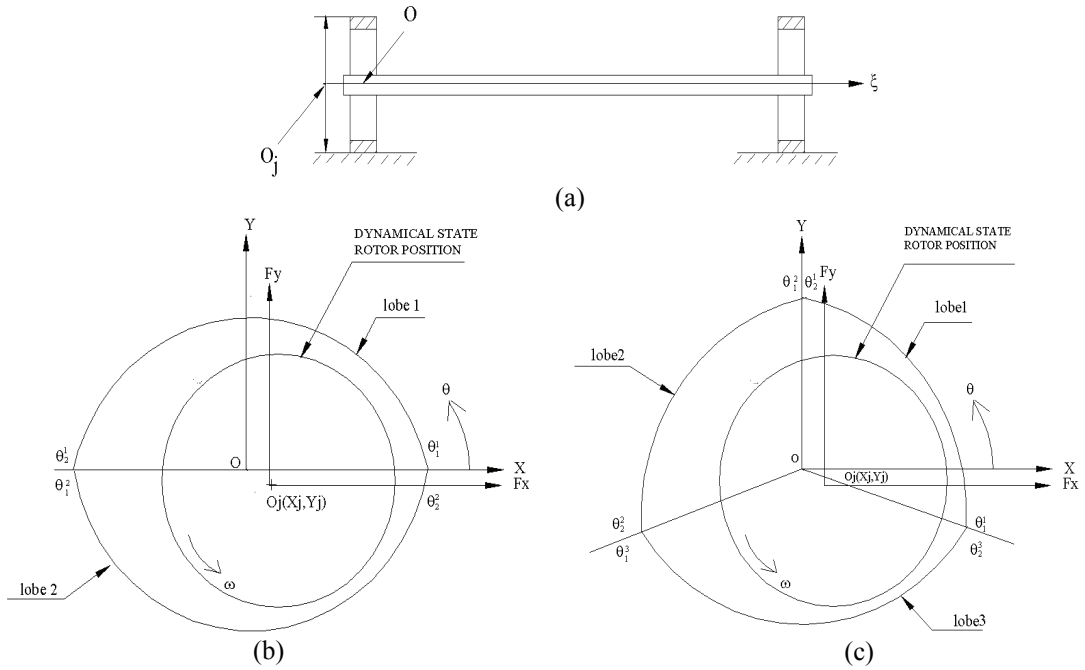

Fig.1. (a) Model of a rigid rotor supported by two aerodynamic noncircular journal bearings, (b) geometric model of two-lobe bearing and (c) geometric model of three-lobe bearing

Due to the nonlinearity of the gas film pressure, it is very difficult to solve the Reynolds equation analytically. Therefore, finite element methods have been employed to obtain the solution and then Runge-Kutta method has been used to solve this equation and equations of motion simultaneously to obtain position, velocity and the acceleration of the rotor center.

2. MATHEMATICAL ANALYSES

a) Governing equations

The geometric details of two types of noncircular bearing configurations are shown in Fig. 1.

Analysis of aerodynamic noncircular bearing involves solution of the governing equations separately for an individual lobe of the bearing, treating each lobe as an independent partial bearing. To generalize the analysis for all noncircular geometries, the film geometry of each lobe is described with reference to bearing fixed Cartesian axes (Fig. 1). Thus, the film thickness in the clearance space of the *k*th lobe, with the rotor in a dynamical state is expressed as [4]:

$$\bar{h} = \bar{C} - (\bar{X}_j)\cos\theta - (\bar{Y}_j)\sin\theta + (\bar{C} - \bar{C}_m)\cos(\theta - \theta_0^k) \tag{1}$$

where $(\bar{X}_j, \bar{Y}_j)$ is the rotor center coordinate in the dynamical state and θ_0^k is angle of lobe line of centers. $\bar{C}$ and $\bar{C}_m$ are conventional radial clearance and minor clearance, when journal and bearing geometric centers are coincident.

The pressure governing equation of isothermal flow field in a bearing lobe is modelled by the Reynolds equation as follows [11]:

$$\frac{\partial}{\partial \bar{X}}\left\{\bar{h}^3 \bar{P}^* \frac{\partial \bar{P}^*}{\partial \bar{X}}\right\} + \frac{\partial}{\partial \bar{Y}}\left\{\bar{h}^3 \bar{P}^* \frac{\partial \bar{P}^*}{\partial \bar{Y}}\right\} = 6\bar{\mu}\left[\bar{U}\frac{\partial}{\partial \bar{X}} + 2\frac{\partial}{\partial \bar{t}}\right](\bar{P}^*\bar{h}) \tag{2}$$

in which $\bar{P}^*$ is the absolute gas pressure, $\bar{\mu}$ is the gas viscosity, $\bar{U}$ is the peripheral speed of the rotor and $\bar{t}$ is the time.

It will be more convenient to express $\bar{P}^*$ as

$$\bar{P}^* = \bar{P}_a + \bar{P} \tag{3}$$

where $\bar{P}_a$ and $\bar{P}$ are the ambient and partial pressure, respectively.

In order to non-dimensionalize Eqs. (1) and (2), let

$$\bar{h} = \bar{C}_m h, \quad \bar{C}_m = \bar{C}\delta, \quad (\bar{X}_j, \bar{Y}_j) = \bar{C}_m (X_j, Y_j), \quad \bar{X} = \bar{R}\theta, \quad \bar{Y} = \bar{R}\xi, \quad \bar{P} = \bar{P}_a P$$
$$\bar{U} = \bar{U}_0 U = \bar{R}\bar{\omega}_0 U, \quad \bar{t} = \frac{\tau}{\bar{\omega}_0}$$

where $\bar{\omega}_0$ is the rotational speed in the steady state and $\bar{R}$ is the rotor radius. Substituting these variables in Eq. (1), the non-dimensional film thickness can be obtained as

$$h = \frac{1}{\delta} - (X_j)\cos\theta - (Y_j)\sin\theta + (\frac{1}{\delta} - 1)\cos(\theta - \theta_0^k) \tag{4}$$

and by substituting Eq. (3) in Eq. (2) and simplifying, the Reynolds equation in non-dimensional form can be expressed as

$$\frac{\partial}{\partial \theta}\left\{h^3(P+1)\frac{\partial P}{\partial \theta}\right\} + \frac{\partial}{\partial \xi}\left\{h^3(P+1)\frac{\partial P}{\partial \xi}\right\} = \Lambda\left[U\frac{\partial}{\partial \theta} + 2\frac{\partial}{\partial \tau}\right]\{(P+1)h\} \tag{5}$$

where θ and ξ are the coordinates in the circumferential and axial directions, respectively and

$$\Lambda = \frac{6\overline{\mu}\overline{\omega}_0\overline{R}^2}{\overline{P}_a\overline{C}_m^2}$$

is the dimensionless parameter called the compressibility number or bearing number.

The Reynolds equation is a nonlinear partial differential equation, therefore, it can be solved using finite element method. For this purpose, let the function variable

$$\Psi = \Psi(\tau) = Ph$$

be introduced into Eq. (5), which then becomes

$$\frac{\partial}{\partial\theta}\left\{h(\Psi+h)\frac{\partial\Psi}{\partial\theta} - (\Psi+h)\Psi\frac{\partial h}{\partial\theta}\right\} + \frac{\partial}{\partial\xi}\left\{h(\Psi+h)\frac{\partial\Psi}{\partial\xi}\right\} = \Lambda\left(U\frac{\partial}{\partial\theta} + 2\frac{\partial}{\partial\tau}\right)(\Psi+h) \tag{6}$$

For the finite element formulation, the Galerkin's weighted residual of Eq. (6) for an element of the discretized space domain of Ψ field is written as

$$\iint_{A^e}\left[\frac{\partial\Psi^e}{\partial t} - \frac{1}{2\Lambda}\frac{\partial}{\partial\theta}\left\{h(\Psi^e+h)\frac{\partial\Psi^e}{\partial\theta} - (\Psi^e+h)\Psi^e\frac{\partial h}{\partial\theta}\right\} - \frac{1}{2\Lambda}\frac{\partial}{\partial\xi}\left\{h(\Psi^e+h)\frac{\partial\Psi^e}{\partial\xi}\right\} + \frac{1}{2}U\frac{\partial}{\partial\theta}(\Psi^e+h) + \frac{\partial h}{\partial\tau}\right]N_i^e\,d\theta d\xi = 0 \tag{7}$$

where N_i^e is an approximation function and A^e is the area of the element. By considering the disccretized domain of Ψ variable and let, in an element 'e', the Ψ function be approximated as

$$\Psi^e = \sum_{j=1}^{n_e} N_j^e\Psi_j(\tau) \tag{8}$$

in which 'e' refers to an element, n_e is the number of nodes in the element, N_j^e's are the shape functions and Ψ_j's are the nodal values of Ψ at time τ. Using Eq. (8) in Eq. (7) and with some integral simplification, the finite element equations for an element of the discretized flow field domain can be obtained as

$$[F]^e\{\dot{\Psi}\}^e = \{V\}^e + \{Q\}^e \tag{9}$$

in which the components of the element matrices are

$$F_{ij}^e = \iint_{A^e} N_i^e N_j^e\,d\theta d\xi \tag{10.1}$$

$$V_i^e = -\frac{1}{2\Lambda}\iint_{A^e}(\Psi^e+h)\left\{h\left(\frac{\partial\Psi^e}{\partial\theta}\frac{\partial N_i^e}{\partial\theta} + \frac{\partial\Psi^e}{\partial\xi}\frac{\partial N_i^e}{\partial\xi}\right) - \left(\Psi^e\frac{\partial h}{\partial\theta} + \Lambda U\right)\frac{\partial N_i^e}{\partial\theta}\right\}d\theta d\xi - \iint_{A^e}\frac{\partial h}{\partial\tau}N_i^e\,d\theta d\xi \tag{10.2}$$

$$Q_i^e = \int_{s^e}(\Psi^e+h)\left\{h\frac{\partial\Psi^e}{\partial\theta} - \Psi^e\frac{\partial h}{\partial\theta} - \Lambda U\right\}N_i^e\,d\xi + \int_{s^e}(\Psi^e+h)h\frac{\partial\Psi^e}{\partial\xi}N_i^e\,d\theta \tag{10.3}$$

where S^e is the boundary of the element.

The assembly of Eq. (8) for all elements of Ψ domain yields the global equations.

$$[F]_{n_f\times n_f}\{\dot{\Psi}\}_{n_f\times 1} = \{V\}_{n_f\times 1} + \{Q\}_{n_f\times 1} \tag{11}$$

where n_f is the total number of nodes and the boundary conditions of the variables for the solution of Eq. (11) are

$$\begin{aligned}
&\Psi\left(\theta_1^k,\zeta,\tau\right)=\Psi\left(\theta_2^k,\zeta,\tau\right)=0\\
&\dot{\Psi}\left(\theta_1^k,\zeta,\tau\right)=\dot{\Psi}\left(\theta_2^k,\zeta,\tau\right)=0\\
&\Psi\left(\theta,\pm\lambda,\tau\right)=0\\
&\dot{\Psi}\left(\theta,\pm\lambda,\tau\right)=0
\end{aligned} \tag{12}$$

At any instant when kinematic state of the rotor center is known, Eq. (11) comprises two variables, Ψ_i and Q_i to be determined. However, at the internal nodes of the discretized space domain, the flux Q_i is zero and Ψ_i is unknown. At the nodes on the boundaries $\xi=\pm\lambda$, and edges of the lobes (θ_1^k and θ_2^k), Ψ_i is known while Q_i is not known. Thus, Eq. (11) really involves as many unknowns as the number of equations and may be solved by invoking the boundary conditions. The solution of these equations yields

$$\left\{\dot{\Psi}\right\}_{n_f\times 1}=\left\{g\right\}_{n_f\times 1} \tag{13}$$

where $g_i=g_i\left(P,\tau\right)$; $i=1,2,...,n_f$

b) Rotor dynamic equations and computation procedure

In the dynamical state, the equations of motion of the rotor can be written as

$$\overline{m}_r\frac{d^2\overline{x}}{d\overline{t}^2}=\left(\overline{F}_X-\overline{F}_{X0}\right) \tag{14}$$

$$\overline{m}_r\frac{d^2\overline{y}}{d\overline{t}^2}=\left(\overline{F}_Y-\overline{F}_{Y0}\right) \tag{15}$$

$\overline{m}_r$ is the mass of rotor and ($\overline{x},\overline{y}$) is the perturbed position of the rotor center that is defined as

$$\overline{x}=\overline{X}_j-\overline{X}_{j0},\overline{y}=\overline{Y}_j-\overline{Y}_{j0} \tag{16}$$

also, ($\overline{F}_X,\overline{F}_Y$) and ($\overline{F}_{X_0},\overline{F}_{Y_0}$) are the components of fluid film force on the rotor in the dynamical and steady states, respectively.

The components of fluid film force on the rotor are given by

$$\begin{Bmatrix}\overline{F}_X-\overline{F}_{X_0}\\ \overline{F}_Y-\overline{F}_{Y_0}\end{Bmatrix}=-\overline{P}_a\overline{R}^2\iint_A\left(P-P_0\right)\begin{Bmatrix}\cos\theta\\ \sin\theta\end{Bmatrix}d\theta d\xi \tag{17}$$

where, A is the pressure area on the rotor, $P_0=\mathrm{P}_0\left(X_{j0},Y_{j0}\right)$ and $P=P\left(X_j,Y_j,V_x,V_y,\tau\right)$ are the film pressure in the steady state and dynamical state, respectively.

The following transformation is introduced

$$x=\overline{x}/\overline{C}_m\,,\ y=\overline{y}/\overline{C}_m$$

and defining non-dimensional groups

$$F_X=\frac{\overline{F}_X}{\overline{P}_a\overline{R}^2},F_{X_0}=\frac{\overline{F}_{X_0}}{\overline{P}_a\overline{R}^2},F_Y=\frac{\overline{F}_Y}{\overline{P}_a\overline{R}^2},F_{Y_0}=\frac{\overline{F}_{Y_0}}{\overline{P}_a\overline{R}^2},m_r=\frac{\overline{m}_r\overline{C}_m\overline{\omega}^2}{\overline{P}_a\overline{R}^2}$$

substituting these non-dimensional groups into Eqs. (14-15) yields

$$A_x=\frac{d^2x}{d\tau^2}=\frac{F_X-F_{X0}}{m_r} \tag{18}$$

$$A_y = \frac{d^2 y}{d\tau^2} = \frac{F_Y - F_{Y0}}{m_r} \tag{19}$$

By defining the state variables

$$S_1 = x, S_2 = y, S_3 = V_x, S_4 = V_y \tag{20}$$

the equations of motion are transformed to the following state space equations as

$$\frac{dS_1}{d\tau} = S_3 \tag{21}$$

$$\frac{dS_2}{d\tau} = S_4 \tag{22}$$

$$\frac{dS_3}{d\tau} = \frac{F_X - F_{X0}}{m_r} \tag{23}$$

$$\frac{dS_4}{d\tau} = \frac{F_Y - F_{Y0}}{m_r} \tag{24}$$

Eqs. (13) and (21-24) describe a nonlinear dynamic system. The equations are restated for convenience

$$\begin{aligned} \frac{dS_i}{d\tau} &= f_i\left(P, S_1, S_2 S_3, S_4, \tau\right) \quad i = 1,2,3,4 \\ \frac{d\Psi_i}{d\tau} &= g_i\left(P, S_1, S_2 S_3, S_4, \tau\right) \quad i = 1,2,\ldots, n_f \end{aligned} \tag{25}$$

The solution procedure commences with an initial static equilibrium state and initial conditions are selected from the static model. Therefore, at the beginning, the Reynolds equation should be solved in the steady state to obtain Ψ_0 and (X_{j0}, Y_{j0}). Meanwhile, the initial velocity of the rotor is assumed to be zero. The numerical integration of Eq. (25) is carried out by the fourth order Runge-Kutta method. By this method, acceleration, velocity and displacement of the rotor are estimated at each time step and are utilized for initial conditions in the next time step. Then, the displacement of the rotor center obtained from each step is used to update the film thickness and the new pressure distribution can be obtained to yield the new dynamical force by integrating it.

3. NUMERICAL STUDIES

Due to the high nonlinearity of gas film forces, the system behavior is studied numerically using the finite element method. In this study, the time step for the calculation is $\pi/300$ and the error tolerance is less than 10^{-6}. The time series data of the first 600000 time steps are excluded from the dynamic behavior investigation to ensure that the data used represent steady state conditions. The resulting data include the orbital paths of the rotor center. These data are then used to generate power spectra, Poincare maps and bifurcation diagrams.

Fast Fourier transformation is used to obtain the power spectra of the rotor center in horizontal and vertical directions.

To generate a Poincare map, a Poincare section that is transverse to the flow of a given dynamic system is considered. The projection of a Poincare section on the $x - y$ plane is related to the Poincare map of the dynamic system. To draw a bifurcation diagram, the obtained points on the Poincare map are used with varying rotor mass by a constant step.

4. RESULTS AND DISCUSSION

In this section, by considering rotor mass as the bifurcation parameter of the system, two different cases of noncircular bearings are studied. The detailed data are as follows [10-11]:

$$\overline{C} = 3\times10^{-5}\, m, \overline{R} = 0.05m, \lambda = 1.5, \delta = 0.6, \overline{\mu} = 1.8\times10^{-5}\,\frac{Kg}{m.s}, \overline{P}_a = 1.013\times10^{5}\,\frac{N}{m^2}$$

To be sure of the proper working of the prepared algorithm, validation of our results has been done in the following manner:

The starting point for analyzing nonlinear dynamic behavior is to determine the static state of the rotor position to be used as the initial condition for the dynamical state. Comparison of these results with those obtained by Chandera, et al. [4] for three-lobe noncircular gas-lubricated journal bearing has been done and shown in Table 1. It is observed that the present results are in good agreement with the reported values in Ref. [4] and justify our work up to this state.

For validation of the results in the dynamical state, the finite difference method has been applied to solve the Reynolds equation and instead of using the Runge-Kutta method, the direct method mentioned in Refs. [10-15] has been considered to obtain acceleration, velocity and displacement of the rotor center. Figure 2 shows the results obtained from the time series data for a three-lobe bearing by two methods where static load and mass of the rotor are chosen to be $\overline{W}_0 = 506.5N$ and $\overline{m}_r = 12.9Kg$, respectively. Also, the bearing number is taken to be $\Lambda = 25$. It is observed that the obtained results with the two methods are in good agreement.

Table 1. Comparison of results in static state for three-lobe noncircular gas bearing

Obtained results by Chandra, et al. (*) $\lambda = 1, \delta = 0.5$					
Λ	W_0	X_{j0}	Y_{j0}	X^*_{j0}	Y^*_{j0}
0.1	0.01	0.217	-0.005	0.223	-0.004
0.5	0.05	0.218	-0.014	0.224	-0.018
1	0.1	0.216	-0.035	0.222	-0.044
2	0.2	0.209	-0.071	0.211	-0.082
5	0.5	0.192	-0.146	0.194	-0.147
10	1	0.212	-0.200	0.212	-0.215
20	2	0.286	-0.324	0.272	-0.323

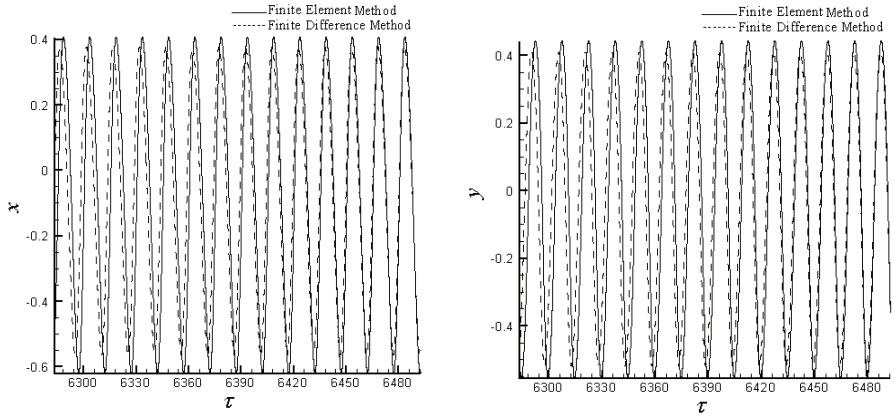

(a) (b)

Fig. 2. Comparison of time series in (a) horizontal and (b) vertical directions calculated by two methods for three-lobe bearing

a) Case 1

Two-lobe noncircular gas bearing is loaded by a static load of $\overline{W_0} = 506.5N$ and the bearing number is taken to be $\Lambda = 25$.

1. Dynamic orbit: Figures 3.1a through 3.4a show the rotor center orbits for different values of the rotor mass. Regular motion is shown at $\overline{m}_r = 15.5$ and $20.65Kg$. But, regular motion loses its stability when the rotor mass is increased to $\overline{m}_r = 28.4$ and $31Kg$. This condition persists for all rotor mass values in the range $28.14 \le \overline{m}_r \le 31.24Kg$.

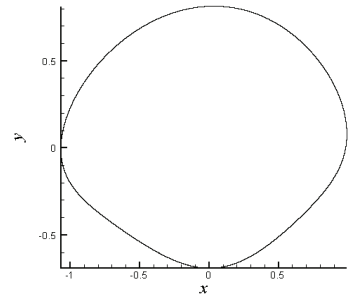

3.1(a)

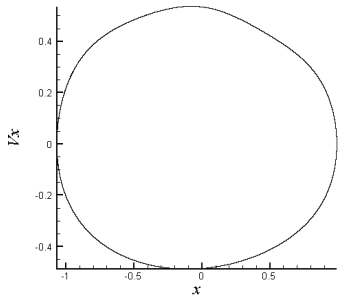

3.1(b)

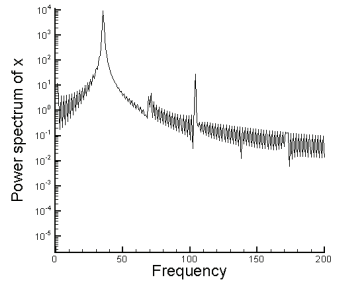

3.1(c)

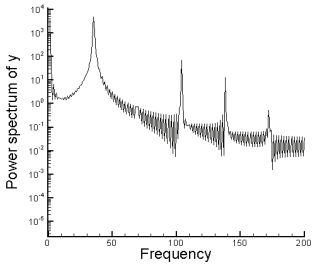

3.1(d)

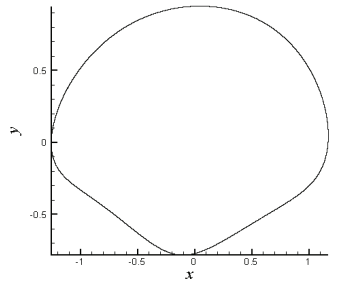

3.2(a)

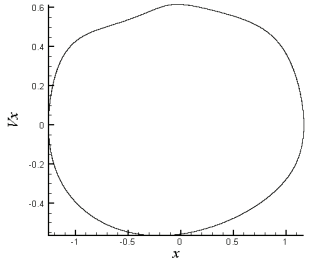

3.2(b)

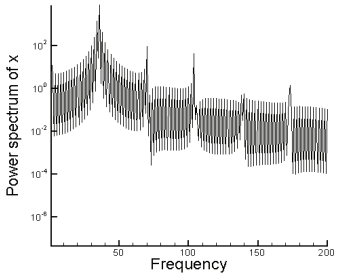

3.2(c)

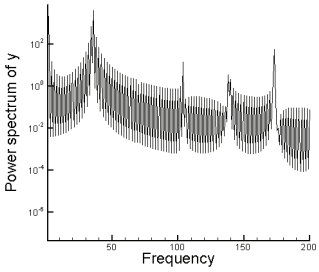

3.2(d)

Fig. 3. Trajectory of the rotor center at $\overline{m}_r = 15.5, 20.65, 28.4, 31Kg$ (3.1(a)-3.4(a)); phase portraits of the rotor center (3.1(b)-3.4(b)) and power spectra of the rotor displacement in the horizontal (3.1(c)-3.4(c)) and vertical (3.1(d)-3.4(d)) directions for two-lobe

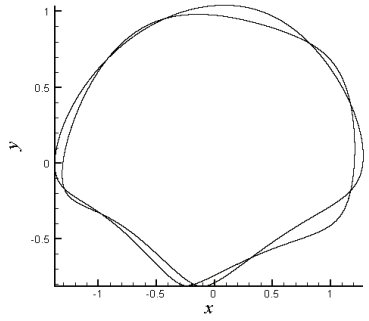

3.3(a)

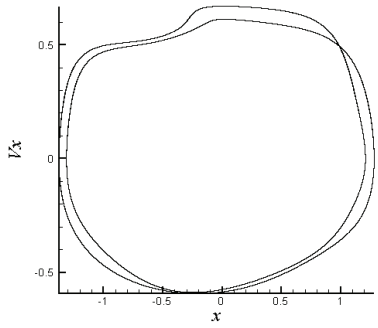

3.3(b)

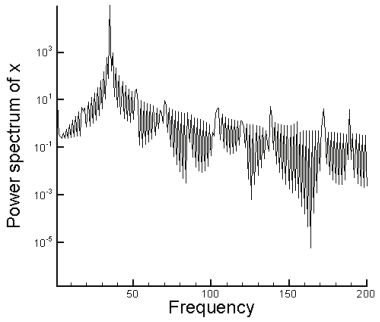

3.3(c)

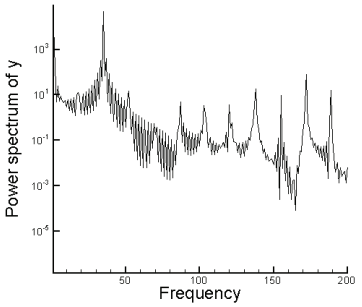

3.3(d)

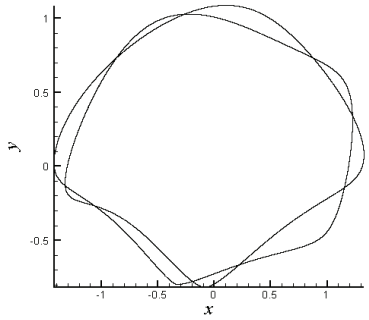

3.4(a)

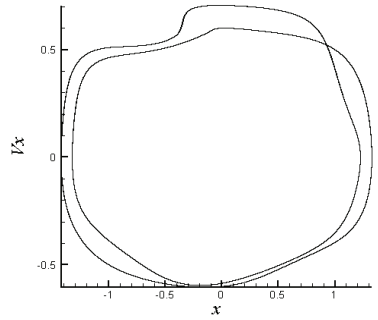

3.4(b)

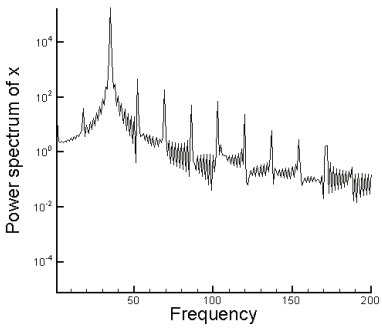

3.4(c)

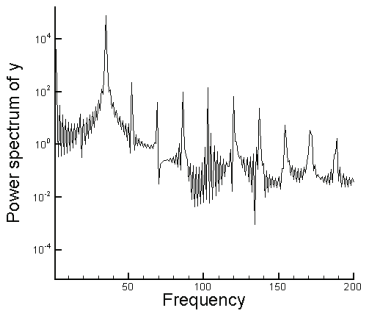

3.4(d)

Fig. 3. Continued

From Figs. 3.1b through 3.4b it is observed that the phase portraits of the rotor center are regular at $\overline{m}_r = 15.5$ and $20.65Kg$ then become irregular at $\overline{m}_r = 28.4$ and $31Kg$.

2. Power spectrum: Figures 3.1c,d through 3.4c,d show the dynamic responses of the rotor center in the horizontal and vertical directions. It is found that the frequency responses of the rotor center demonstrate

harmonic motion for the rotor mass values of $\overline{m}_r = 15.5$ and $20.65Kg$ in both directions. But, they become KT-periodic motion at $\overline{m}_r = 28.4$ and $31Kg$.

3. Bifurcation diagram and Poincare map: Bifurcation diagram is a useful means to observe nonlinear dynamic behavior. By considering rotor mass value as a parameter of the system, qualitatively different behavior can be observed in Fig. 4 at the range of $10 \le \overline{m}_r \le 32Kg$.

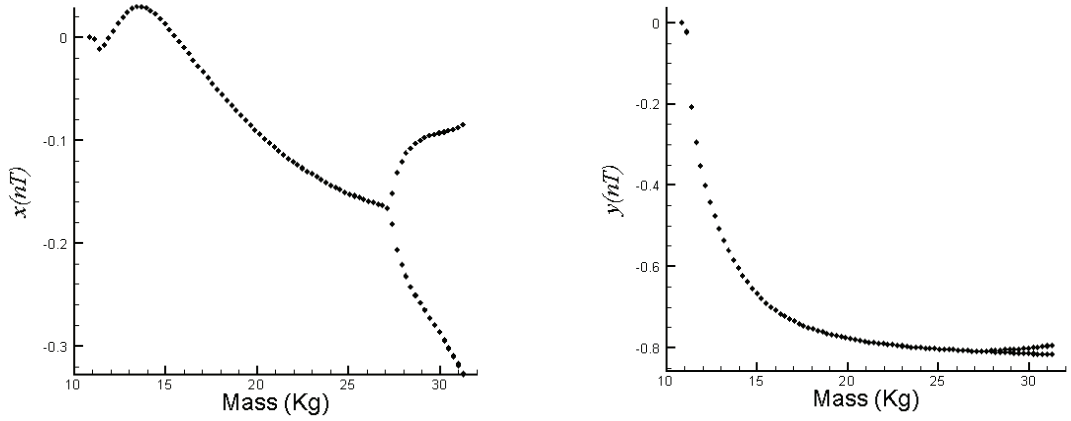

(a) (b)

Fig. 4. Bifurcation diagrams: (a) $x(nT)$ and (b) $y(nT)$ versus rotor mass for two-lobe bearing

Results show that, before $\overline{m}_r = 10.84Kg$, the system returns to equilibrium position of the rotor center in the static state. However, the system has periodic motion in the horizontal and vertical directions at the range of $10.84 \le \overline{m}_r \prec 28.14Kg$. Figures 5a and b show the Poincare maps at $\overline{m}_r = 15.5$ and $20.65Kg$. One point on these maps confirms T-periodic motion of the rotor in both directions. It can be observed that $2T$-periodic motion occurs in the interval of $28.14 \le \overline{m}_r \le 31.24Kg$. The Poincare maps at $\overline{m}_r = 28.4$ and $31Kg$ are shown in Figs. 5c and d. Two discrete points on these maps demonstrate $2T$-periodic motion of the rotor center at these values of rotor mass. When the rotor mass value exceeds 31.24*Kg*, contact between the rotor and bearing would occur.

b) Case 2

In the second case, a three-lobe noncircular gas bearing is loaded by a static load of $\overline{W}_0 = 506.5N$ and the bearing number is taken to be $\Lambda = 25$.

1. Dynamic orbit: Figures 6.1a through 6.4a show the rotor center orbits at different values of the rotor mass. Regular motion is shown at $\overline{m}_r = 15.5$ and $31Kg$. But, regular motion loses its stability when the rotor mass is increased to $\overline{m}_r = 36.14$ and $36.4Kg$. This condition persists for all rotor mass values in the range $36.14 \le \overline{m}_r \le 36.92Kg$.

From Figs. 6.1b through 6.4b it is observed that the phase portraits of the rotor center are regular at $\overline{m}_r = 15.5$ and $31Kg$ then become irregular at $\overline{m}_r = 36.14$ and $36.4Kg$.

2. Power spectrum: Figures 6.1c,d through 6.4c,d show the dynamic responses of the rotor center in the horizontal and vertical directions. It is found that the frequency responses of the rotor center demonstrate harmonic motion for the rotor mass values $\overline{m}_r = 15.5$ and $31Kg$ in both directions, but they become KT-periodic motion at $\overline{m}_r = 36.14$ and $36.4Kg$.

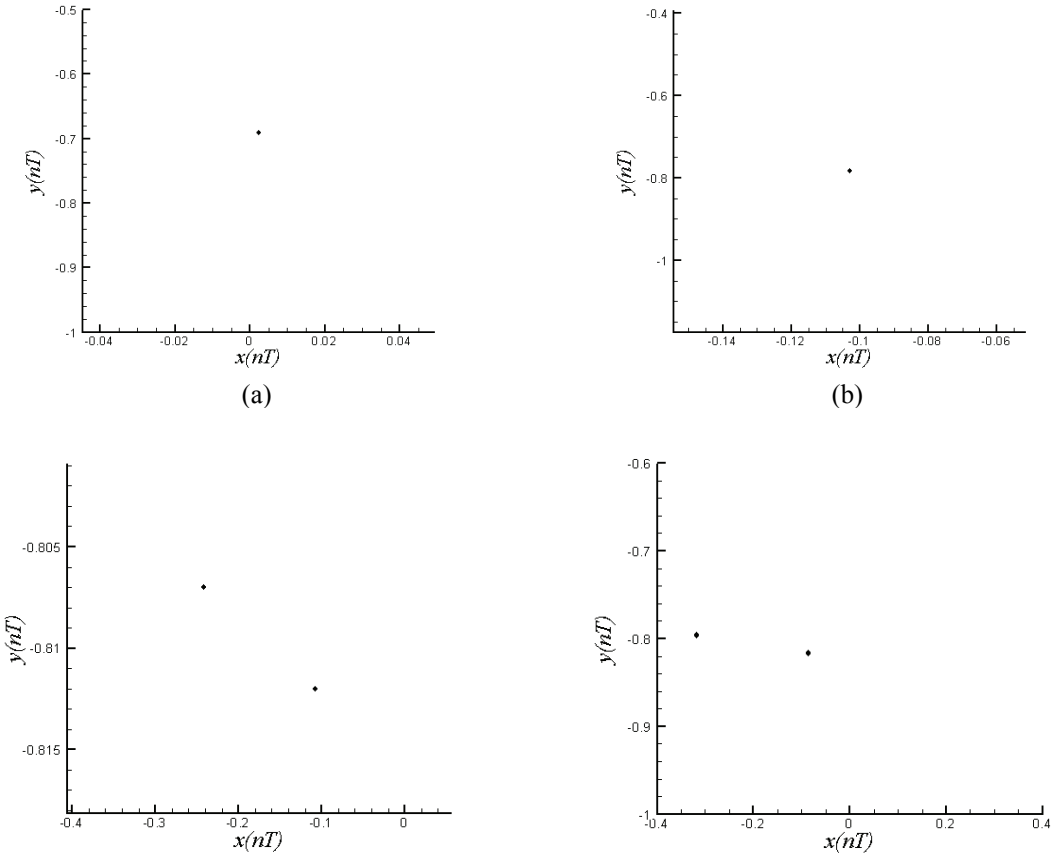

Fig. 5. Poincare maps of the rotor center trajectory at (a) $\overline{m}_r = 15.5$, (b) 20.65, (c) 28.4, (d) 31*Kg*

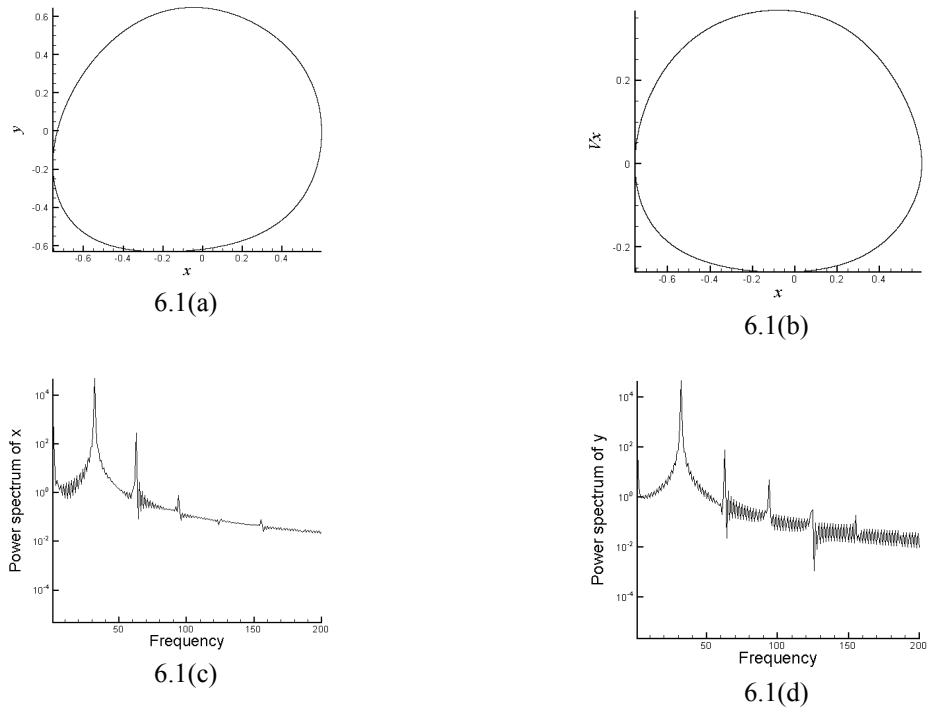

Fig. 6. Trajectory of the rotor center at $\overline{m}_r = 15.5$, 31, 36.14 and 36.4 *Kg* (6.1(a)-6.5(a)); phase portraits of the rotor center (5.1(b)-5.5(b)) and power spectra of the rotor displacement in the horizontal (6.1(c)-6.5(c)) and vertical (6.1(d)-6.5(d)) directions for three-lobe bearing

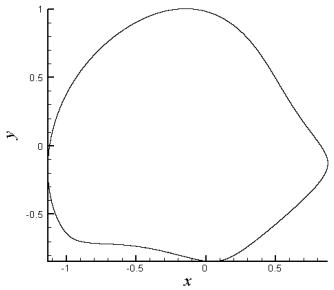

6.2(a)

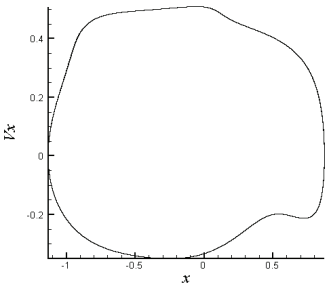

6.2(b)

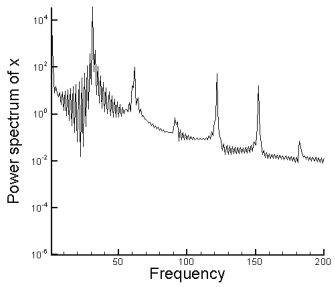

6.2(c)

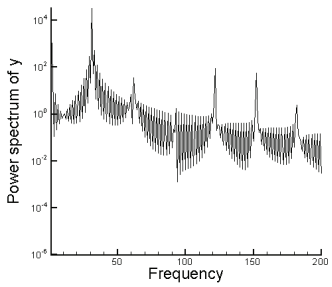

6.2(d)

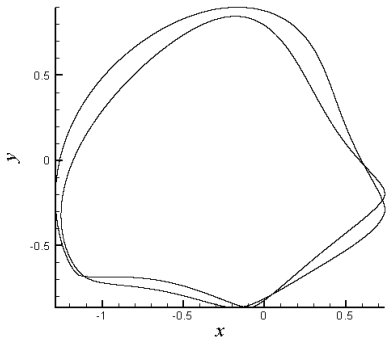

6.3(a)

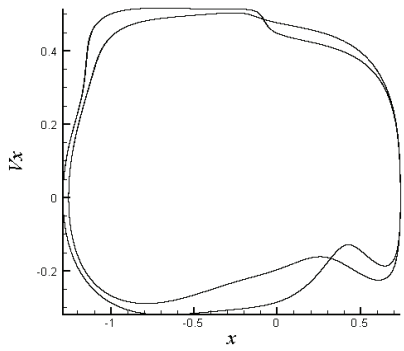

6.3(b)

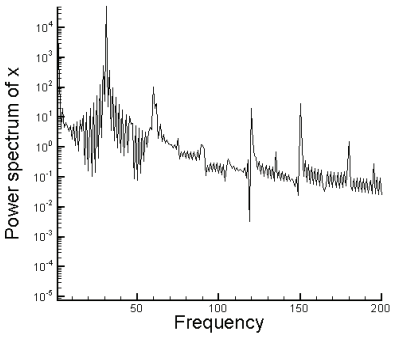

6.3(c)

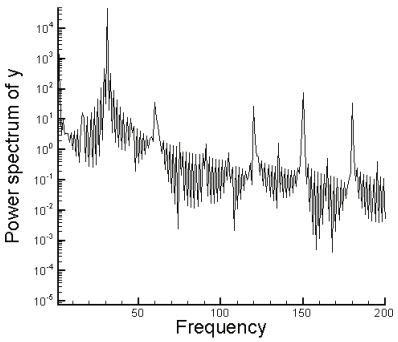

6.3(d)

Fig. 6. Continued

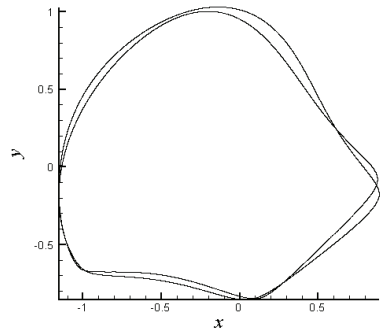

6.4(a)

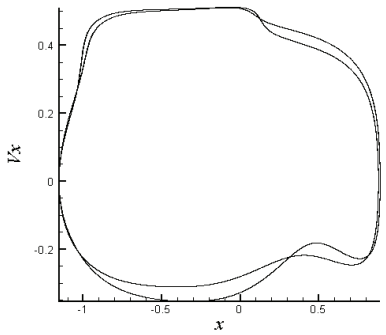

6.4(b)

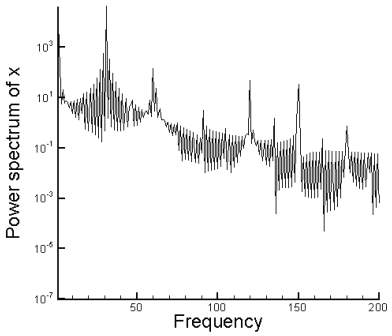

6.4(c)

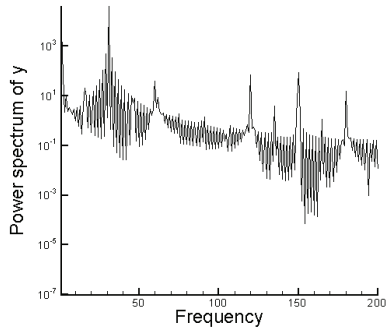

6.4(d)

Fig. 6. Continued

3. Bifurcation diagram and Poincare map: By considering rotor mass value as a parameter of the system, qualitatively different behavior can be observed in Fig. 7 at the range of $10 \le \overline{m}_r \le 38Kg$.

Results show that, before $\overline{m}_r = 11.87Kg$, the system returns to the equilibrium position of the rotor center in the static state, but at the range of $11.87 \le \overline{m}_r \prec 35.36Kg$ the system has periodic motion in the horizontal and vertical directions. Figures 8a and b show the Poincare maps at $\overline{m}_r = 15.5$ and $31Kg$, respectively. One point on these maps confirms T-periodic motion of the rotor in both directions. It can be seen that $2T$-periodic motion occurs in the interval of $35.36 \le \overline{m}_r \prec 36.4Kg$. The Poincare map at $\overline{m}_r = 36.14$ is shown in Fig. 8c and two points on this map demonstrate this behavior. But, in the interval of $36.4 \le \overline{m}_r \prec 36.92Kg$, $3T$ periodic motion appears and Fig. 8d confirms this behavior at $\overline{m}_r = 36.4Kg$. When rotor mass value becomes $36.92Kg$ contact between the rotor and bearing would occur.

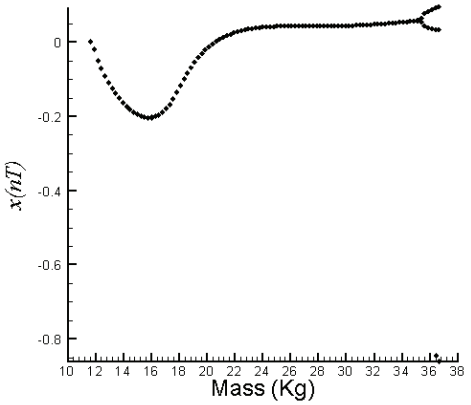

(a)

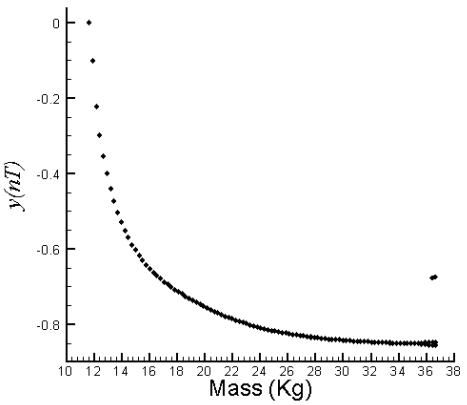

(b)

Fig. 7. Bifurcation diagrams: (a) $x(nT)$ and (b) $y(nT)$ versus rotor mass for three-lobe bearing

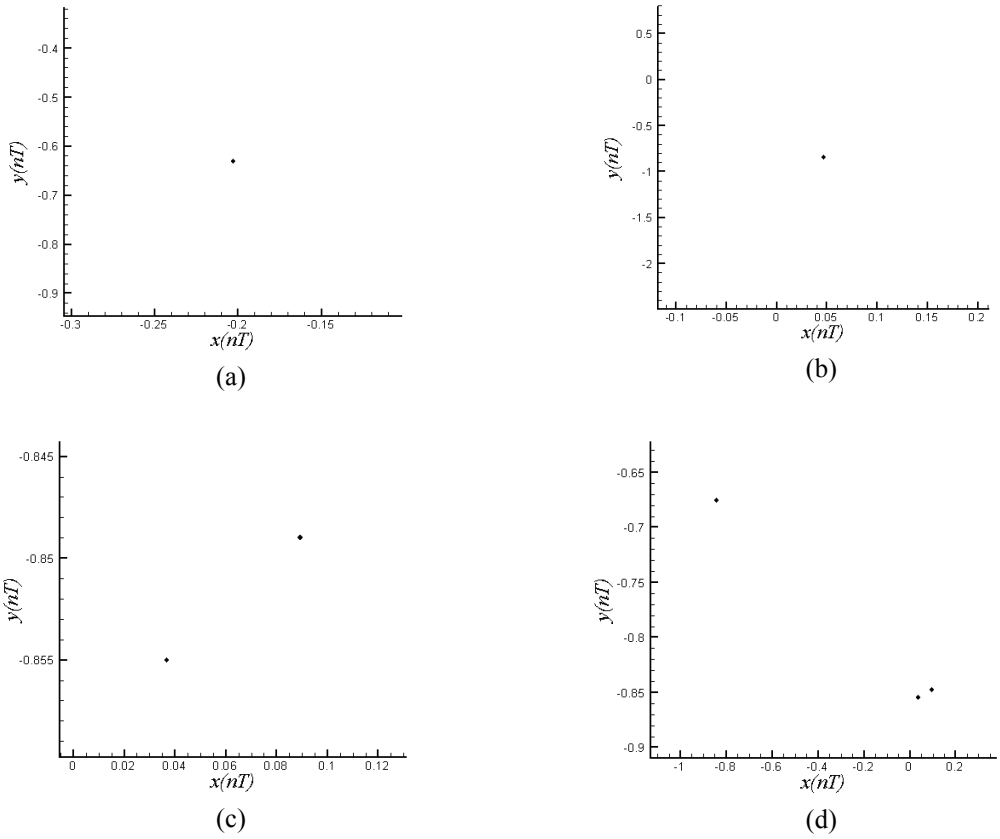

Fig. 8. Poincare maps of the rotor center trajectory at (a) $\overline{m}_r = 15.5$, (b) 31, (c) 36.14, (d) 36.4Kg

5. CONCLUSION

The effect of rotor mass on nonlinear dynamic behavior of a rigid rotor supported by noncircular aerodynamic journal bearings has been studied in this study. Two types of noncircular bearings such as two and three-lobe bearings have been considered. Due to nonlinearity of the gas film force, computational methods have been employed to study the dynamical behavior of the system. Dynamical orbits, power spectra, Poincare maps and bifurcation diagrams are used to identify the dynamic behavior of these systems.

From this study, it is shown that by considering rotor mass as a parameter of the system, return to equilibrium position of the rotor center in the static state, periodic and KT-periodic motions and contact between rotor and bearing occur in both two and three-lobe bearings. By comparing two types of the considered bearings, it can be seen that at the same conditions, three-lobe bearing has better dynamical performance than two-lobe bearing.

The variation of this parameter plays a major role in noncircular bearing systems. Thus, by selecting the proper type of bearing and changing the system parameter to suitable values, the rotor center can avoid undesirable behavior.

NOMENCLATURE

$\overline{C}$	conventional radial clearance, (m)
$\overline{C}_m$	minor clearance when rotor and bearing geometric centers are coincident, (m)
$\overline{D}$	rotor diameter, (m)

$\overline{F}_{X_0}, \overline{F}_{Y_0}$ components of the fluid film force on the rotor in the steady state, (N)

$\overline{F}_X, \overline{F}_Y$ components of the fluid film force on the rotor in the dynamical state, (N)

$\overline{W}_0$ static load, (N)

$\overline{h}$ film thickness, (m)

$\overline{L}$ bearing length, (m)

$\overline{m}_r$ rotor mass, (Kg)

N_i shape function

n_e number of nodes in an element

n_f number of nodes in fluid domain

$\overline{P}^*$ absolute gas pressure, ($\frac{N}{m^2}$)

$\overline{P}$ partial gas pressure, ($\frac{N}{m^2}$)

$\overline{P}_a$ ambient pressure, ($\frac{N}{m^2}$)

$\overline{R}$ rotor radius, (m)

$\overline{t}$ time, (s)

$\overline{U}$ peripheral speed of the rotor in dynamical state, ($\frac{m}{s}$)

$\overline{X}, \overline{Y}$ cartesian axes with origin at the bearing geometric center, (m)

$\overline{X}_{j0}, \overline{Y}_{j0}$ coordinates of the rotor center in steady state, (m)

$\overline{X}_j, \overline{Y}_j$ coordinates of the rotor center in dynamical state, (m)

$\overline{x}, \overline{y}$ perturbation coordinates of the rotor center measured from its static equilibrium position, (m)

V_x, V_y dimensionless velocity of the rotor center in horizontal and vertical directions

A_x, A_y dimensionless acceleration of the rotor center in horizontal and vertical directions

δ preload in the bearing, ($\frac{\overline{C}_m}{\overline{C}}$)

λ bearing aspect ratio, ($\frac{\overline{L}}{\overline{D}}$)

Λ bearing number

$\overline{\mu}$ ambient dynamic viscosity of the lubricant, ($\frac{N.s}{m^2}$)

θ angular coordinate measured from X – axis

θ_0^k angle of lobe line of centers

θ_1^k, θ_2^k angles at the leading and trailing edge of the lobe

$\overline{\omega}$ rotational speed of the rotor, ($\frac{rad}{s}$)

τ dimensionless time

$\overline{\xi}$ coordinate along bearing axis measured from mid span, (m)

superscripts

e element numbers

k lobe designation

subscript

0	static equilibrium position of the rotor bearing at $\tau = 0$

REFERENCES

1. Castelli, V. & Elrod, H. G. (1961). Solution of the stability problem for 360 degree self-acting, gas-lubricated bearing. *ASME J. Basic Eng.*, Vol. 87, pp. 199-212.
2. Ausman, J. S. (1963). Linearized PH stability theory for translatory half-speed whirl of long self-acting gas-lubricated journal bearings. *ASME J. Basic Eng.*, Vol. 83, pp. 611-619.
3. Holmes, A. G., Ettles, C. M. & Mayes, I. W. (1978). Aperiodic behavior of a rigid shaft in short journal bearings. *Int. J. Numeric. Method Eng.*, Vol. 12, pp. 695-702.
4. Chandra, M., Malik, M. & Sinhasan, R. (1983). Comparative study of four gas-lubricated noncircular journal bearing configuration. *Tribology Int.*, Vol. 16, pp. 103-108.
5. Zhao, J. Y., Linnentt, I. W. & Melean, L. J. (1994). Subharmonic and quasi-periodic motion of an eccentric squeeze film damper-mounted rigid rotor. *ASME J. Vib. Acoust*., Vol. 116, pp. 357-363.
6. Adiletta, G., Guido, A. R. & Rossi, C. (1996). Chaotic motion of a rigid rotor in short journal bearings. *Nonlinear Dyn.*, Vol. 10, pp. 251-269.
7. Adiletta, G., Guido, A. R. & Rossi, C. (1997). Nonlinear dynamics of rigid unbalanced rotor in short bearings. Part I: Theoretical Analysis. *Nonlinear Dyn.*, Vol. 14, pp. 57-87.
8. Adiletta, G., Guido, A. R. & Rossi, C. (1997). Nonlinear dynamics of rigid unbalanced rotor in short bearings. Part II: Experimental Analysis. *Nonlinear Dyn.*, Vol. 14, pp. 157-189.
9. Czolczynski, K. & Kapitaniak, T. (1997). Hopf bifurcation in rotors supported in gas bearings. *Chaos, Solitons & Fractals*, Vol. 4, pp. 499-515.
10. Wang, C. C. & Chen, C. K. (2001). Bifurcation analysis of self-acting gas journal bearings. *J. Tribilogy, 123*, pp. 755-767.
11. Wang, C. C., Jang, M. J. & Chen, C. K. (2004). Nonlinear dynamic analysis of a flexible rotor supported by self-acting gas journal bearing. *Proceedings of the Inst. of Mech. Eng.*, Vol. 12, pp. 1527-538.
12. Wang, J. S. & Wang, C. C. (2005). Nonlinear dynamic and bifurcation analysis of short aerodynamic journal bearings. *Tribology Int*., Vol. 38, pp. 740-748.
13. Wang, C. C. (2006). Nonlinear dynamic behavior and bifurcation analysis of a rigid rotor supported by relatively short externally pressurized porous gas journal bearing system. *Acta Mech.*, Vol. 183, 41-60.
14. Wang, C. C. (2007). Bifurcation analysis of an aerodynamic journal bearing system considering the effect of stationary herringbone grooves. *Chaos, Solitons & Fractal*, Vol. 33, Vol. 1532-1545.
15. Wang, C. C., Yau, H. T., Jang, M. J. & Yeh, Y. L. (2007). Theoretical analysis of the non-linear behavior of a flexible rotor supported by herringbone grooved gas journal bearings. *Tribology Int.*, Vol. 40, pp. 533-541.
16. Rahmatabadi, A. D. & Rashidi, R. (2006). Effect of mount angle on static and dynamic characteristics of gas-lubricated, noncircular journal bearings. *Iranian. Journal of Science & Technology, Transaction B, Engineering*, Vol. 37, pp. 27-37.
17. Rahmatabadi, A. D. & Rashidi, R. (2007). Investigation of preload effects on noncircular gas bearing systems performance. *JAST*, Vol. 4, pp. 33-38.